

Role of signal degradation in directional chemosensing

Ryan LeFebre,¹ Joseph A. Landsittel,^{1,2} David E. Stone,³ and Andrew Mugler^{1,*}

¹*Department of Physics and Astronomy, University of Pittsburgh, Pittsburgh, Pennsylvania 15260, USA*

²*Department of Mathematics, University of Pittsburgh, Pittsburgh, Pennsylvania 15260, USA*

³*Department of Biological Sciences, University of Illinois at Chicago, Chicago, IL 60607, USA*

Directional chemosensing is ubiquitous in cell biology, but some cells such as mating yeast paradoxically degrade the signal they aim to detect. While the data processing inequality suggests that such signal modification cannot increase the sensory information, we show using a reaction-diffusion model and an exactly solvable discrete-state reduction that it can. We identify a non-Markovian step in the information chain allowing the system to evade the data processing inequality, reflecting the nonlocal nature of diffusion. Our results apply to any sensory system in which degradation couples to diffusion. Experimental data suggest that mating yeast operate in the beneficial regime where degradation improves sensing.

Cells actively alter their environment by secreting chemical factors. In many cases, environmental alteration by secretion of a degrading factor or by other means allows cells to form their own directional gradients out of uniform chemical backgrounds [1]. Examples include epithelial cell migration [2], lymphocyte targeting [3], embryogenesis [4], metastatic invasion [2, 5], and chemotactic bacteria [6, 7]. On the other hand, some cases are known in which a gradient is already present, and yet cells secrete a degrading factor anyway. A well-studied example is the chemotropic mating response of the budding yeast, *Saccharomyces cerevisiae* [8].

Haploid budding yeast cells come in two mating types. Each type secretes an attracting pheromone that is sensed by the partner type. Paradoxically, each type also secretes an enzyme that degrades the pheromone of the opposite type. Thus, a chemical gradient that each cell can use for directional sensing is already present, and yet the cell actively degrades it. It is known that this degradation is vital for efficient mating [9, 10], but the reasons are not completely understood. It has been proposed that yeast releases this degrading enzyme to disambiguate partner locations [11], prevent pheromone receptor saturation [8], and to sharpen the gradient of the pheromone profile [8, 12, 13].

Here, we focus on the role of degradation in sharpening the pheromone gradient because it raises a general question about the acquisition of sensory information. In principle, sharpening a gradient is useful for directional sensing, but in this case, it is achieved by the removal of pheromone. This removal will lower the overall concentration profile, which in turn should increase the sensory noise. If the disadvantage of increased noise outweighs the advantage of sharpening the gradient, degrading the signal may not actually be beneficial for sensing. In fact, the data processing inequality states that information cannot be increased by locally post-processing a signal [14], which would seem to disfavor this strategy. This brings us to the central question of this paper: Is it ever beneficial for a sensory system to destroy a signal it is trying to detect?

We investigate this question using a model that accounts for molecule secretion, diffusion, and sensing by a spherical source and spherical detector. Using a perturbative approach, and accounting for diffusive fluctuations in the concentration profile, we arrive at an analytical expression for the detector’s signal-to-noise ratio. As expected, we find that degradation sharpens the gradient, but it also increases noise. Taken together, the signal-to-noise ratio increases with degradation, revealing a successful sensing strategy that is nonetheless in apparent violation of data processing inequality.

To understand this apparent violation, we reduce the model to a set of discrete states where we can calculate the mutual information between the source and detector exactly. The reduced model pinpoints a key non-Markovian step in the sensory process. Because the data processing inequality assumes Markovianity, this finding explains how the inequality is evaded. Our analysis suggests that the nonlocal character of diffusion is responsible for the information gain due to degradation. We interpret our results in terms of yeast mating but also in terms of sensory problems in general.

Consider two spheres—a source and a detector—a distance r_0 apart (Fig. 1A). These spheres have radius a and can represent whole cells themselves or, in the case of mating yeast, specific macromolecular complexes on the cell surfaces called “gradient tracking machines” [15]. The source releases, at rate ν , an attracting pheromone with diffusion coefficient D_c , while the detector releases, at rate μ , a degrading enzyme with diffusion coefficient D_b . The pheromone is degraded by the enzyme with rate k_d . Calling the concentrations of pheromone and enzyme c and b , respectively, the dynamics are

$$\dot{b} = D_b \nabla^2 b \quad (1)$$

$$\dot{c} = D_c \nabla^2 c - k_d bc. \quad (2)$$

In steady-state, Eq. 1 is solved by $b = \mu / (4\pi D_b |\vec{r} - r_0 \hat{z}|)$ in a coordinate system centered on the source (Fig. 1A). Non-dimensionalizing with $\rho \equiv r/a$ and $\chi \equiv ca^3$, Eq. 2

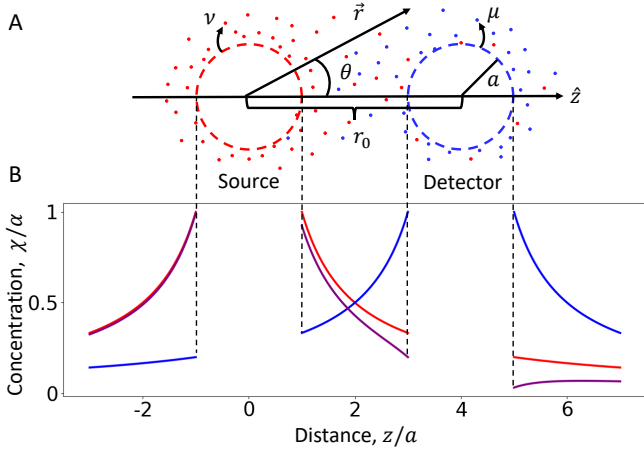


FIG. 1. Model and concentration profiles. (A) A spherical source secretes a diffusing pheromone that is degraded by a diffusing enzyme secreted by a spherical detector. (B) The pheromone profile (Eq. 4) along the z axis without (red, $\varepsilon = 0$) and with (purple, $\varepsilon = 0.2$) degradation for separation $\rho_0 = r_0/a = 4$. The enzyme profile scales inversely with distance from the detector (blue).

in steady state then becomes

$$\nabla^2 \chi = \frac{\varepsilon}{|\vec{\rho} - \rho_0 \vec{z}|} \chi, \quad (3)$$

where $\varepsilon \equiv ak_a \mu / (4\pi D_b D_c)$ is a dimensionless parameter that reflects the strength of degradation.

Because Eq. S9 has a $\vec{\rho}$ -dependent coefficient, it is not immediately solvable by linear transform methods. Therefore, we use a perturbation approach, treating ε as a small parameter (an assumption we later relax when simplifying the model to a set of discrete states). Specifically, writing $\chi = \chi_0 + \varepsilon \chi_1$, the zeroth-order term satisfying $\nabla^2 \chi_0 = 0$ is $\chi_0 = \alpha / \rho$, where $\alpha \equiv \nu a^2 / (4\pi D_c)$ is a dimensionless parameter that reflects the strength of pheromone release. We solve for the first order term satisfying $\nabla^2 \chi_1 = \varepsilon \chi_0 / |\vec{\rho} - \rho_0 \vec{z}|$ by expanding in spherical harmonics (see Supplemental Material). The result is

$$\chi = \frac{\alpha}{\rho} - \varepsilon \alpha \sum_{\ell=0}^{\infty} P_{\ell}(\cos \theta) \left[\frac{\ell(2\ell+1)\rho_0 - \ell}{(\ell+1)(2\ell+1)\rho_0^{\ell+1}\rho^{\ell+1}} + \frac{\rho_{<}^{\ell}}{\rho_{>}^{\ell}} - \frac{\rho_{<}^{\ell+1}}{(2\ell+2)\rho_{>}^{\ell+1}} - \frac{1}{(2\ell+1)(2\ell+2)\rho_{<}^{\ell+1}\rho_{>}^{\ell+1}} \right], \quad (4)$$

where P_{ℓ} are the Legendre polynomials, and $\rho_{<}$ ($\rho_{>}$) represents the lesser (greater) of ρ and ρ_0 . Eq. 4 is plotted in Fig. 1B (purple), and we see that degradation by the enzyme (blue) results in a pheromone profile that is depleted near the detector relative to that without the enzyme present (red).

We see in Fig. 1B that degradation sharpens the pheromone gradient at the detector in the direction of the source [16]. Most eukaryotic cells, including yeast,

do not actually measure the local gradient in a particular direction (the way that, say, motile bacteria do by moving along it [17]). Rather, they compare detection events at many locations on their surface [18]. The order parameter that captures this comparison is the anisotropy [19–21],

$$A = \frac{\int d\tilde{\Omega} \chi(1, \tilde{\theta}) \cos \tilde{\theta}}{\int d\tilde{\Omega}' \chi(1, \tilde{\theta}')}, \quad (5)$$

where $\chi(\tilde{\rho}, \tilde{\theta})$ is Eq. 4 transformed to coordinates centered at the detector (with $\tilde{\theta} = 0$ pointing at the source), and $d\tilde{\Omega} = \sin \tilde{\theta} d\tilde{\theta} d\phi$ is the corresponding solid angle element. The cosine performs the comparison, such that $A > 0$ ($A < 0$) corresponds to gradients toward (away from) the source. To evaluate the integrals in Eq. 5, we use a planar approximation $\chi(\tilde{\rho}, \tilde{\theta}) = c_1 + c_2 \tilde{z}$ for the concentration profile, where the coefficients c_1 and c_2 are given by Eq. 4 at the detector surface (see Supplemental Material). Eq. 5 then evaluates to

$$A = \frac{2 + \varepsilon(G - F)(\rho_0^2 - 1)}{3[2\rho_0 - \varepsilon(F + G)(\rho_0^2 - 1)]}, \quad (6)$$

where F and G are functions of ρ_0 (see Supplemental Material) that satisfy $G - F > 0$ when source and detector do not overlap ($\rho_0 > 2$). Eq. 6 is plotted in Fig. 2 (blue), and we see that the anisotropy A increases with the degradation strength ε , consistent with the sharpening of the gradient.

Eq. 6 represents the detected signal but not the noise. To calculate the noise, we add Langevin terms to Eqs. 1 and 2 whose strengths are determined intrinsically by the

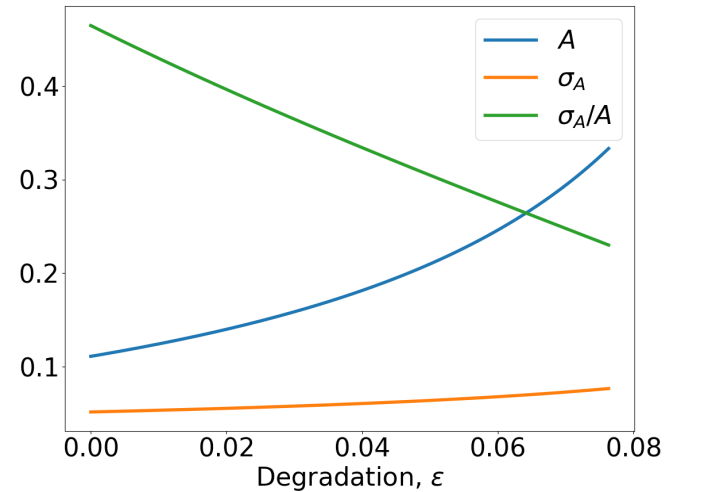


FIG. 2. The anisotropy A (Eq. 6, blue) and its time-averaged variance σ_A^2 (Eq. 7, orange) both increase with the dimensionless degradation parameter $\varepsilon = ak_a \mu / (4\pi D_b D_c)$ for small ε . The ratio σ_A/A (green) decreases, indicating a beneficial sensing strategy. Parameters are $\rho_0 = 3$, and $\nu T = 3000$.

parameters, and that contain the spatiotemporal correlations appropriate for diffusion [19, 21] (see Supplemental Material). Fourier transforming these equations obtains the power spectrum for A , whose low-frequency limit is $T\sigma_A^2$, where σ_A^2 is the variance in the long-time average of the anisotropy, and T is the averaging time. The result is

$$\sigma_A^2 = \frac{2(\rho_0^2 - 1)}{3\nu T} \left\{ 1 + \varepsilon \left[\frac{(F + G)(\rho_0^2 - 1)}{\rho_0} - \frac{3}{5} \right] \right\}. \quad (7)$$

Intuition for this result can be gained from the following scaling argument. The anisotropy in Eq. 5 should scale as $A \sim \Delta n / \bar{n}$, where $\Delta n = n_2 - n_1$ is the front-to-back difference in the number of detected molecules, and $n = n_2 + n_1$ is their sum [22, 23]. The variance in the anisotropy should then scale as $\sigma_{\Delta n}^2 / \bar{n}^2 \approx \sigma_n^2 / \bar{n}^2$, where the second step neglects the cross-correlations between n_2 and n_1 . The variance in the time-averaged anisotropy is further reduced by the number T/τ of independent measurements made in the averaging time T , where τ is the correlation time; hence $\sigma_A^2 \sim \sigma_n^2 / (\bar{n}^2 T / \tau)$. With diffusion and degradation, the statistics of the number of molecules in a given volume is Poissonian, $\sigma_n^2 = \bar{n}$, and the correlation time is set by the sum of rates set by diffusion and degradation. The diffusion rate is D_c/a^2 , while inspection of Eq. 2 reveals an effective degradation rate of $k_d b$. Evaluating b near the detector surface gives $b = \mu / (4\pi D_b a)$, and therefore a correlation time of $\tau = [D_c/a^2 + k_d \mu / (4\pi D_b a)]^{-1} = a^2 / [D_c(1 + \varepsilon)]$. Thus, $\sigma_A^2 \sim a^2 / [\bar{n} D_c (1 + \varepsilon) T]$, or recalling that $\alpha = \nu a^2 / (4\pi D_c)$, we have $\sigma_A^2 \sim \alpha / [\bar{n} \nu (1 + \varepsilon) T]$. Obtaining \bar{n} by integrating the concentration profile in Eq. 4 over the volume of the detector, $\bar{n} = \int d^3 \tilde{\rho} \chi(\rho, \theta)$, and again using the planar approximation for χ as above, we find that this expression for σ_A^2 recovers Eq. 7 up to numerical factors of order unity (see Supplemental Material).

Eq. 7 is plotted in Fig. 2 (orange), and we see that the noise σ_A increases with the degradation strength ε . This result is consistent with the idea that degradation reduces the molecule number \bar{n} , which increases the noise as $\sigma_A \sim 1/\sqrt{\bar{n}}$ as shown above. However, we also see in Fig. 2 that the ratio σ_A/A of the noise to the signal decreases with the degradation strength ε (green). This result reveals that the benefit of increased signal outweighs the detriment of increased noise, such that the signal-to-noise ratio A/σ_A still increases with degradation. Such a result would seem to be in violation of the data processing inequality, since processing (i.e., degrading) the signal has increased the sensory information (i.e., the signal-to-noise ratio).

To resolve this paradox, we reduce our model to a set of discrete states, allowing us to solve for the sensory information exactly. The simplification will be considerable but will preserve all ingredients (secretion, diffusion, and degradation) and therefore the basic physics.

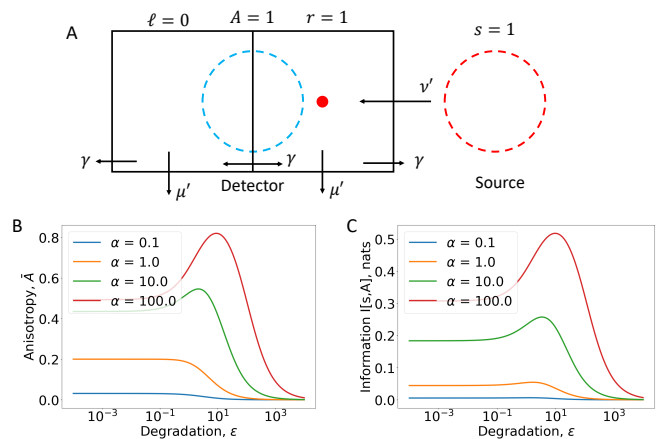


FIG. 3. Discrete-state reduction. (A) Locations left and right of the detector contain either zero or one pheromone molecule. Transition rates accounting for secretion, diffusion, and degradation map to the dimensionless parameters α and ε of the full model. (B) Average anisotropy \bar{A} (right-left occupancy difference). (C) Mutual information between A and source location s (left or right). Both measures increase, then decrease, with degradation parameter ε .

Furthermore, it will have the added benefit that ε is no longer confined to be small. Specifically, we reduce the spatial domain to two locations, one on either side of the detector, each of which may contain either zero or one pheromone molecule (Fig. 3A). The source is on one side or the other and secretes pheromone at that location. Pheromone diffuses between locations or out of the system, and is degraded. Thus, the sensory problem is reduced to: how much information does the difference in pheromone occupancies give about the source direction (left or right)?

To answer this question, we seek the conditional probability $p_{\ell r | s}$, where the binary variables $\ell \in \{0, 1\}$ and $r \in \{0, 1\}$ represent the left and right pheromone occupancies, and the binary variable $s \in \{-1, 1\}$ represents the left-right location of the source. Calling ν' , γ , and μ' the secretion, diffusion, and degradation rates, respectively (Fig. 3A), the dynamics of $p_{\ell r | s}$ are

$$\begin{aligned} \dot{p}_{00|1} &= (\gamma + \mu')(p_{01|1} + p_{10|1}) - \nu' p_{00|1} \\ \dot{p}_{01|1} &= \nu' p_{00|1} + \gamma p_{10|1} + (\gamma + \mu') p_{11|1} - (2\gamma + \mu') p_{01|1} \\ \dot{p}_{10|1} &= \gamma p_{01|1} + (\gamma + \mu') p_{11|1} - (\nu' + 2\gamma + \mu') p_{10|1} \\ \dot{p}_{11|1} &= \nu' p_{10|1} - 2(\gamma + \mu') p_{11|1}, \end{aligned} \quad (8)$$

and a similar set of equations for $s = -1$ [24]. The rates ν' , γ , and μ' can be mapped to their counterparts in the unreduced model as follows. The effective pheromone degradation rate is $\mu' = k_d b = k_d \mu / (4\pi D_b a)$ as reasoned above. Diffusion across the detector happens at a rate on the order of $\gamma = D_c/a^2$. We thus have $\mu'/\gamma = a k_d \mu / (4\pi D_b D_c) = \varepsilon$, naturally recovering the dimensionless degradation strength within the reduced model. The effective secretion rate ν' is reduced

from ν according to the distance of the detector from the source. For convenience we define $\nu' = \nu/(4\pi)$, such that $\nu'/\gamma = \alpha$, with the understanding that in general this ratio would be inversely related to ρ_0 . In terms of these rate ratios, the steady state of Eq. 8 reads

$$\begin{aligned} p_{00|1} &= (1 + \varepsilon)^2(6 + 2\varepsilon + \alpha)/Z, & p_{10|1} &= 2(1 + \varepsilon)\alpha/Z, \\ p_{01|1} &= (1 + \varepsilon)\alpha(4 + 2\varepsilon + \alpha)/Z, & p_{11|1} &= \alpha^2/Z, \end{aligned} \quad (9)$$

where $Z \equiv (2 + 2\varepsilon + \alpha)[3 + 2\alpha + \varepsilon(4 + \varepsilon + \alpha)]$.

In the reduced model, the anisotropy is equivalent to the difference in pheromone occupancies, $A = r - \ell$. Noting the simple relationship between $p_{A|s}$ and $p_{\ell r|s}$ [25], the average anisotropy $\bar{A} \equiv \langle A|s = 1 \rangle$ follows from Eq. 9 as

$$\bar{A} = \frac{\alpha(1 + \varepsilon)}{3 + 2\alpha + \varepsilon(4 + \varepsilon + \alpha)}. \quad (10)$$

Eq. 10 is plotted in Fig. 3B, and we see that the anisotropy \bar{A} increases with degradation strength ε for small ε , as in the unreduced model (Fig. 2, blue). For large ε , the anisotropy ultimately vanishes, as it must for a completely degraded signal. Thus, an optimal degradation strength ε_* emerges that scales as $\varepsilon_* \sim \sqrt{\alpha}$ for large α .

The analog of the signal-to-noise ratio is the sensory information: the mutual information [26] between s and A ,

$$\begin{aligned} I[s; A] &= \sum_{sA} p_{A|s} p_s \log \frac{p_{A|s}}{\sum_{s'} p_{A|s'} p_{s'}} \\ &= \frac{2\alpha(1 + \varepsilon)}{Z} \left(\beta \log \frac{2\beta}{\beta + 1} + \log \frac{2}{\beta + 1} \right), \end{aligned} \quad (11)$$

where $\beta \equiv 2 + \varepsilon + \alpha/2$. Here, the second step assumes the detector has no initial knowledge of the source direction ($p_s = 1/2$), inserts $p_{A|s}$ from Eq. 9, and simplifies. Eq. 11 is plotted in Fig. 3C, and we see that the information, like the anisotropy, increases and then decreases with ε . In particular, the increase shows that the reduced model reproduces the apparent violation of the data processing inequality.

Importantly, the reduced model allows us to explain the apparent violation. The information flow in the system is as follows: the source direction informs the pheromone profile, the pheromone profile is degraded, and the degraded profile informs the anisotropy. Denoting the four-state pheromone profile (ℓ, r) as q without degradation, and as q' with degradation, this flow implies the chain $s \rightarrow q \rightarrow q' \rightarrow A$. If this chain is Markovian, i.e., $p_{sqq'A} = p_s p_{q|s} p_{q'|q} p_{A|q'}$, then the data processing inequality implies $I[s; q] \geq I[s; q'] \geq I[s; A]$. In the Supplemental Material we prove that $I[s; q'] \geq I[s; A]$ holds but that $I[s; q] \geq I[s; q']$ does not. The latter implies that the piece of the chain $s \rightarrow q \rightarrow q'$ is non-Markovian, meaning that q' is not conditionally independent of s

given q . In other words, the degraded profile q' carries more information about the source direction s than is contained in the unmodified profile q .

Why is the chain $s \rightarrow q \rightarrow q'$ non-Markovian? The reason is that degradation, when coupled to diffusion, is not a local modification to the signal. That is, when a molecule within the profile is degraded, the rest of the profile does not remain the same. Instead, diffusion reshuffles the profile, filling in the gaps to create a new steady state. This reshuffling occurs because the steady state is non-equilibrium: flux in from secretion is balanced elsewhere by flux out from diffusion and degradation. The resulting steady state is then entirely different from, and evidently more informative than, the unmodified one, despite the fact that molecules are lost.

These insights also extend to systems that form a gradient out of a uniform background. A particularly simple example is the synthesis-diffusion-degradation model of morphogenesis [27, 28], in which molecules enter from one side of an embryo, diffuse, and spontaneously degrade. Without degradation, diffusion would make the profile tend toward uniform. Degradation instead makes the profile fall off away from the source. Degradation thus introduces a gradient, which provides cell nuclei their positional information, despite destroying the signal that they detect.

What are the implications of our findings for mating yeast? Mating partners are typically no more than a few cell radii away, meaning that the optimal degradation condition for nearby cells, $\varepsilon_* \approx \sqrt{\alpha}$ (Fig. 3B, C), applies. If degradation is to improve sensing, we therefore must have $\varepsilon < \sqrt{\alpha}$, or, inserting the expressions for ε and α and ignoring factors of order unity, $\mu < (D_b/k_d)\sqrt{D_c\nu}$. Note that the source or detector radius a drops out of this condition, so that it does not matter for what follows whether sensing is performed by the entire cell or a local macromolecular complex. In mating yeast, the pheromone is α -factor, which is secreted by a source cell at a rate of $\nu \approx 1350$ molecules per second in the presence of a mating partner [29]. The enzyme is Bar1, which binds to α -factor with a second-order rate of $k_d = 7.7 \mu\text{M}^{-1}\text{s}^{-1} = 0.013 \mu\text{m}^3/\text{s}$ [30]. Estimating the diffusion coefficients $D_c = 125 \mu\text{m}^2/\text{s}$ and $D_b = 6 \mu\text{m}^2/\text{s}$ from the molecules' weights [8], the condition becomes $\mu < 140\nu$. Although we are unaware of measurements of the secretion rate μ of Bar1, it is unlikely that it exceeds a hundred times that of the pheromone. Therefore, our analysis predicts that mating yeast orient toward their partners under conditions in which signal degradation helps, rather than hurts, sensory precision.

We have demonstrated that degrading a directional signal can be beneficial for detecting that signal because the advantage of sharpening the gradient outweighs the disadvantage of signal loss. We have argued that this benefit is possible, despite the implications of the data processing inequality, because diffusion makes the sig-

nal modification nonlocal. The net result is an optimal level of signal degradation: enough to amplify the directional information, but not too much to destroy the signal entirely. Comparing our findings with experimental data suggests that mating yeast operate in the beneficial regime where degradation amplifies the information. Our predictions are generic and apply to any directional sensing system in which signal degradation is employed to shape or reshape a diffusive gradient.

We thank Ming Chen, Bard Ermentrout, and Bill Bialek for helpful discussions. This work was supported by National Science Foundation grant numbers PHY-2118561 and MCB-2003415.

* andrew.mugler@pitt.edu

- [1] Luke Tweedy, Olivia Susanto, and Robert H Insall. Self-generated chemotactic gradients—cells steering themselves. *Current opinion in cell biology*, 42:46–51, 2016.
- [2] Cally Scherber, Alexander J Aranyosi, Birte Kulemann, Sarah P Thayer, Mehmet Toner, Othon Iliopoulos, and Daniel Irimia. Epithelial cell guidance by self-generated egf gradients. *Integrative Biology*, 4(3):259–269, 2012.
- [3] Susan R Schwab and Jason G Cyster. Finding a way out: lymphocyte egress from lymphoid organs. *Nature immunology*, 8(12):1295–1301, 2007.
- [4] Erika Donà, Joseph D Barry, Guillaume Valentin, Charlotte Quirin, Anton Khmelinskii, Andreas Kunze, Sevi Durdu, Lionel R Newton, Ana Fernandez-Minan, Wolfgang Huber, et al. Directional tissue migration through a self-generated chemokine gradient. *Nature*, 503(7475):285–289, 2013.
- [5] Andrew J Muinonen-Martin, Olivia Susanto, Qifeng Zhang, Elizabeth Smethurst, William J Faller, Douwe M Veltman, Gabriela Kalna, Colin Lindsay, Dorothy C Bennett, Owen J Sansom, et al. Melanoma cells break down lpa to establish local gradients that drive chemotactic dispersal. *PLoS biology*, 12(10):e1001966, 2014.
- [6] Xiongfei Fu, Setsu Kato, Junjia Long, Henry H Mattingly, Caiyun He, Dervis Can Vural, Steven W Zucker, and Thierry Emonet. Spatial self-organization resolves conflicts between individuality and collective migration. *Nature communications*, 9(1):2177, 2018.
- [7] Jonas Cremer, Tomoya Honda, Ying Tang, Jerome Wong-Ng, Massimo Vergassola, and Terence Hwa. Chemotaxis as a navigation strategy to boost range expansion. *Nature*, 575(7784):658–663, 2019.
- [8] Meng Jin, Beverly Errede, Marcelo Behar, Will Mather, Sujata Nayak, Jeff Hasty, Henrik G Dohlman, and Timothy C Elston. Yeast dynamically modify their environment to achieve better mating efficiency. *Science signaling*, 4(186):ra54–ra54, 2011.
- [9] Russell K Chan and Carol A Otte. Physiological characterization of *saccharomyces cerevisiae* mutants supersensitive to g1 arrest by a factor and α factor pheromones. *Molecular and cellular biology*, 2(1):21–29, 1982.
- [10] Catherine L Jackson and Leland H Hartwell. Courtship in *s. cerevisiae*: both cell types choose mating partners by responding to the strongest pheromone signal. *Cell*, 63(5):1039–1051, 1990.
- [11] Naama Barkai, Mark D Rose, and Ned S Wingreen. Protease helps yeast find mating partners. *Nature*, 396(6710):422–423, 1998.
- [12] Steven S Andrews, Nathan J Addy, Roger Brent, and Adam P Arkin. Detailed simulations of cell biology with smoldyn 2.1. *PLoS computational biology*, 6(3):e1000705, 2010.
- [13] Vinal Lakhani and Timothy C Elston. Testing the limits of gradient sensing. *PLoS Computational Biology*, 13(2):e1005386, 2017.
- [14] Joy A. Thomas and Thomas M. Cover. *Elements of information theory*. John Wiley & Sons, 1999.
- [15] Xin Wang, Wei Tian, Bryan T Banh, Bethanie-Michelle Statler, Jie Liang, and David E Stone. Mating yeast cells use an intrinsic polarity site to assemble a pheromone-gradient tracking machine. *Journal of Cell Biology*, 218(11):3730–3752, 2019.
- [16] We also see in Fig. 1B that degradation can reverse the gradient in the direction away from the source. Because the anisotropy measure we adopt in the text integrates over the entire detector surface, it accounts for the pheromone profile in all directions, including away from the source.
- [17] Howard C Berg. *Random walks in biology*. Princeton University Press, 1993.
- [18] Robert A Arkowitz. Responding to attraction: chemotaxis and chemotropism in dictyostelium and yeast. *Trends in cell biology*, 9(1):20–27, 1999.
- [19] Sean Fancher, Michael Vennettilli, Nicholas Hilgert, and Andrew Mugler. Precision of flow sensing by self-communicating cells. *Physical review letters*, 124(16):168101, 2020.
- [20] Robert G Endres and Ned S Wingreen. Accuracy of direct gradient sensing by single cells. *Proceedings of the National Academy of Sciences*, 105(41):15749–15754, 2008.
- [21] Julien Varennes, Sean Fancher, Bumsoo Han, and Andrew Mugler. Emergent versus individual-based multicellular chemotaxis. *Phys. Rev. Lett.*, 119:188101, 2017.
- [22] Michael Vennettilli, Louis González, Nicholas Hilgert, and Andrew Mugler. Autologous chemotaxis at high cell density. *Phys. Rev. E*, 106:024413, Aug 2022.
- [23] Andrew Mugler, Andre Levchenko, and Ilya Nemenman. Limits to the precision of gradient sensing with spatial communication and temporal integration. *Proceedings of the National Academy of Sciences*, 113(6):E689–E695, 2016.
- [24] Specifically, $p_{00|1} = p_{00|-1}$, $p_{01|1} = p_{10|-1}$, $p_{10|1} = p_{01|-1}$, and $p_{11|1} = p_{11|-1}$.
- [25] Specifically, the relationship between $p_{A|s}$ and $p_{E|s}$ is $p_{-1|s} = p_{10|s}$, $p_{0|s} = p_{00|s} + p_{11|s}$, and $p_{1|s} = p_{01|s}$.
- [26] Claude Elwood Shannon. A mathematical theory of communication. *The Bell system technical journal*, 27(3):379–423, 1948.
- [27] Ortrud Wartlick, Anna Kicheva, and Marcos González-Gaitán. Morphogen gradient formation. *Cold Spring Harbor perspectives in biology*, 1(3):a001255, 2009.
- [28] Thomas Gregor, Eric F Wieschaus, Alistair P McGregor, William Bialek, and David W Tank. Stability and nuclear dynamics of the bicoid morphogen gradient. *Cell*, 130(1):141–152, 2007.
- [29] David W Rogers, Ellen McConnell, and Duncan Greig. Molecular quantification of *saccharomyces cerevisiae* α -pheromone secretion. *FEMS yeast research*, 12(6):668–

674, 2012.

[30] Stephen K Jones Jr, Starlynn C Clarke, Charles S Craik, and Richard J Bennett. Evolutionary selection on bar-

rier activity: Bar1 is an aspartyl protease with novel substrate specificity. *MBio*, 6(6):10–1128, 2015.

SUPPLEMENTAL MATERIAL

Pheromone and Enzyme Concentrations

Denoting the concentration of the degrading enzyme and attractant pheromone as b and c respectively, the equations for their diffusion and interaction are as in Eqs. 1 and 2 of the main text,

$$\dot{b} = D_b \nabla^2 b \quad (\text{S1})$$

$$\dot{c} = D_c \nabla^2 c - k_d b c. \quad (\text{S2})$$

Working in steady-state, it is easy to solve the equation for the degrading enzyme while centered on the detector:

$$D_b \nabla^2 b(r, \theta, \phi) = 0 \quad (\text{S3})$$

$$b(r, \theta, \phi) = \sum_{\ell=0}^{\infty} \sum_{m=-\ell}^{\ell} \left(A_{\ell m} r^{\ell} + B_{\ell m} r^{-\ell-1} \right) Y_{\ell m}(\theta, \phi), \quad (\text{S4})$$

where $Y_{\ell m}$ are spherical harmonics. Noting the spherical symmetry of the problem ($l = m = 0$) and using the boundary condition of $b \rightarrow 0$ as $r \rightarrow \infty$, Eq. S4 becomes

$$b = \frac{B}{r}. \quad (\text{S5})$$

B is to be determined from the boundary condition involving the release of the enzyme through the surface of the cell

$$-4\pi a^2 D_b \left(\frac{\partial b}{\partial r} \right)_{r=a} = \mu. \quad (\text{S6})$$

This gives the solution to b

$$b(r) = \frac{\mu}{4\pi D_b r}. \quad (\text{S7})$$

Shifting the coordinate system to be centered on the source, Eq. S7 becomes

$$b(r) = \frac{\mu}{4\pi D_b |\vec{r} - r_0 \vec{z}|}. \quad (\text{S8})$$

Still working in steady-state, non-dimensionalizing with $\rho \equiv r/a$ and $\chi \equiv ca^3$, and using Eq. S8, Eq. S2 becomes

$$\nabla^2 \chi = \frac{\varepsilon}{|\vec{\rho} - \rho_0 \vec{z}|} \chi, \quad (\text{S9})$$

where $\varepsilon \equiv ak_d \mu / (4\pi D_b D_c)$ is a dimensionless parameter that reflects the strength of degradation. Equation S9 has a variable coefficient and therefore it is not immediately solvable by linear transform methods. We proceed using perturbation theory for small ε ,

$$\chi = \chi_0 + \varepsilon \chi_1 + \dots \quad (\text{S10})$$

Plugging Eq. S10 into Eq. S9 and matching terms up to first order we have

$$\nabla^2 \chi_0 = 0 \quad (\text{S11})$$

$$\nabla^2 \chi_1 = \frac{\varepsilon}{|\vec{\rho} - \rho_0 \vec{z}|} \chi_0. \quad (\text{S12})$$

The boundary conditions for χ are as follows:

$$\chi(\rho \rightarrow \infty) = 0, \quad (\text{S13})$$

which gives

$$\chi_0(\rho \rightarrow \infty) = 0, \quad (\text{S14})$$

$$\chi_1(\rho \rightarrow \infty) = 0. \quad (\text{S15})$$

The boundary condition at the surface of the cell is

$$-4\pi a^{-2} D_c \left(\frac{\partial \chi}{\partial \rho} \right)_{\rho=1} = \nu. \quad (\text{S16})$$

Rewriting $\alpha = \nu a^2 / 4\pi D_c$, we have

$$\left(\frac{\partial \chi_0}{\partial \rho} \right)_{\rho=1} + \varepsilon \left(\frac{\partial \chi_1}{\partial \rho} \right)_{\rho=1} = -\alpha. \quad (\text{S17})$$

χ_0 is the concentration of the pheromone when there is no enzyme present. Therefore, Eq. S17 gives,

$$\left(\frac{\partial \chi_0}{\partial \rho} \right)_{\rho=1} = -\alpha, \quad (\text{S18})$$

$$\left(\frac{\partial \chi_1}{\partial \rho} \right)_{\rho=1} = 0. \quad (\text{S19})$$

Using the boundary conditions it is easy to solve Eq. S11,

$$\chi_0 = \frac{\alpha}{\rho}. \quad (\text{S20})$$

The equation for χ_1 now becomes

$$\nabla^2 \chi_1 = \frac{\alpha}{|\vec{\rho}'| |\vec{\rho} - \rho_0 \vec{z}'|}. \quad (\text{S21})$$

The solution to χ_1 is the sum of the homogenous χ_1^h , and particular χ_1^p solutions. We will solve the particular solution using a Green's function,

$$\chi_1^p = \alpha \int d^3 \rho' \frac{G(\rho, \rho')}{|\vec{\rho}'| |\vec{\rho} - \rho_0 \vec{z}'|}. \quad (\text{S22})$$

The Green's function of the Laplace operator is

$$G(\rho, \rho') = \frac{-1}{4\pi |\vec{\rho} - \vec{\rho}'|} = \sum_{\ell=0}^{\infty} \frac{-1}{4\pi} \frac{\rho_{<}^{\ell}}{\rho_{>}^{\ell+1}} P_{\ell}(\cos \gamma) \quad (\text{S23})$$

where γ is the angle between the two vectors, $\rho_{>} = \max(\rho, \rho')$, $\rho_{<} = \min(\rho, \rho')$, and P_{ℓ} is the Legendre polynomial. The Legendre polynomial can be expanded in terms of spherical harmonics

$$P_{\ell}(\cos(\gamma)) = \frac{4\pi}{2\ell+1} \sum_{m=-\ell}^{\ell} Y_{\ell m}^*(\theta', \phi') Y_{\ell m}(\theta, \phi). \quad (\text{S24})$$

Plugging Eqs. S23 and S24 into Eq. S22 we get

$$\chi_1^p = -\alpha \int d^3 \rho' \frac{1}{\rho'} \left(\sum_{\ell m} \frac{\rho_{<}^{\ell}}{\rho_{>}^{\ell+1} (2\ell+1)} Y_{\ell m}^*(\theta', \phi') Y_{\ell m}(\theta, \phi) \right) \left(\sum_{\ell'} \frac{\rho_{0<}^{\ell'}}{\rho_{0>}^{\ell'+1}} \sqrt{\frac{4\pi}{2\ell'+1}} Y_{\ell' 0}(\theta^*) \right). \quad (\text{S25})$$

Here, $\rho'_{0>} = \max(\rho', \rho_0)$ and $\rho'_{0<} = \min(\rho', \rho_0)$. Equation S25 can be simplified using the orthogonality relationship of the spherical harmonics

$$\int d\Omega' Y_{\ell m}^*(\theta, \phi) Y_{\ell' m'}(\theta, \phi) = \delta_{\ell\ell'} \delta_{mm'}. \quad (\text{S26})$$

Rearranging the integral in Eq. S25 into radial and angular parts and then using Eq. S26, Eq. S25 becomes

$$\chi_1^p = -\alpha \sum_{\ell=0}^{\infty} \frac{\sqrt{4\pi}}{(2\ell+1)^{3/2}} Y_{\ell 0}(\theta) \int_1^{\infty} d\rho' \rho' \frac{\rho_{<}^{\ell}}{\rho_{>}^{\ell+1}} \frac{\rho'_{0<}^{\ell}}{\rho'_{0>}^{\ell+1}}. \quad (\text{S27})$$

The integral in Eq. S27 depends on whether ρ is greater than or less than ρ_0 .

$$\int_1^{\infty} d\rho' \rho' \frac{\rho_{<}^{\ell}}{\rho_{>}^{\ell+1}} \frac{\rho'_{0<}^{\ell}}{\rho'_{0>}^{\ell+1}} = \int_1^{\rho} d\rho' \frac{\rho'^{2\ell+1}}{(\rho\rho_0)^{\ell+1}} + \int_{\rho}^{\rho_0} d\rho' \frac{\rho^{\ell}}{\rho_0^{\ell+1}} + \int_{\rho_0}^{\infty} d\rho' \frac{(\rho\rho_0)^{\ell}}{\rho'^{2\ell+1}} \quad \rho < \rho_0 \quad (\text{S28})$$

$$\int_1^{\infty} d\rho' \rho' \frac{\rho_{<}^{\ell}}{\rho_{>}^{\ell+1}} \frac{\rho'_{0<}^{\ell}}{\rho'_{0>}^{\ell+1}} = \int_1^{\rho_0} d\rho' \frac{\rho'^{2\ell+1}}{(\rho\rho_0)^{\ell+1}} + \int_{\rho_0}^{\rho} d\rho' \frac{\rho_0^{\ell}}{\rho^{\ell+1}} + \int_{\rho}^{\infty} d\rho' \frac{(\rho\rho_0)^{\ell}}{\rho'^{2\ell+1}} \quad \rho > \rho_0. \quad (\text{S29})$$

Solving the integrals in Eqs. S28 and S29 and writing the solution in terms of Legendre polynomials, the particular solution is

$$\chi_1^p = -\alpha \sum_{\ell=0}^{\infty} \frac{P_{\ell}(\cos\theta)}{2\ell+1} \left[(2\ell+1) \left(\frac{\rho_{<}}{\rho_{>}} \right)^{\ell} - \frac{2\ell+1}{2\ell+2} \left(\frac{\rho_{<}}{\rho_{>}} \right)^{\ell+1} - \frac{1}{(2\ell+2)(\rho_{<}\rho_{>})^{\ell+1}} \right], \quad (\text{S30})$$

where $\rho_{>}$ and $\rho_{<}$ are $\max(\rho, \rho_0)$ and $\min(\rho, \rho_0)$ respectively. The homogenous solution is the fundamental solution to Laplace's equation with azimuthal symmetry,

$$\chi_1^h = \sum_{\ell=0}^{\infty} \left(A_{\ell} \rho^{\ell} + B_{\ell} \rho^{-\ell-1} \right) P_{\ell}(\cos\theta). \quad (\text{S31})$$

Applying the boundary condition from Eq. S15 means that $A_{\ell} = 0$ for all ℓ ,

$$\chi_1^h = \sum_{\ell=0}^{\infty} \left(\frac{B_{\ell}}{\rho^{\ell+1}} \right) P_{\ell}(\cos\theta). \quad (\text{S32})$$

The B_{ℓ} can be solved for using the remaining boundary condition, Eq. S19,

$$0 = -\sum_{\ell=0}^{\infty} B_{\ell}(\ell+1) P_{\ell}(\cos\theta) - \alpha \sum_{\ell=0}^{\infty} \frac{P_{\ell}(\cos\theta)}{2\ell+1} \left[\frac{\ell}{\rho_0^{\ell}} \left(2\ell+1 - \frac{1}{\rho_0} \right) \right] \quad (\text{S33})$$

$$B_{\ell} = \frac{-\alpha \ell (2\ell+1 - 1/\rho_0)}{(\ell+1)(2\ell+1)\rho_0^{\ell}}. \quad (\text{S34})$$

Putting it all together we have,

$$\chi = \frac{\alpha}{\rho} - \varepsilon \left[\alpha \sum_{\ell}^{\infty} P_{\ell}(\cos\theta) \left(\frac{\ell(2\ell+1 - 1/\rho_0)}{(\ell+1)(2\ell+1)\rho_0^{\ell}\rho^{\ell+1}} + \left(\frac{\rho_{<}}{\rho_{>}} \right)^{\ell} - \frac{1}{(2\ell+2)} \left(\frac{\rho_{<}}{\rho_{>}} \right)^{\ell+1} - \frac{1}{(2\ell+1)(2\ell+2)(\rho_{<}\rho_{>})^{\ell+1}} \right) \right], \quad (\text{S35})$$

as in Eq. 4 of the main text.

Anisotropy

To solve for the anisotropy, A , it is beneficial to shift the coordinate system to be centered on the detector. In this system, $\tilde{\rho}$ and $\tilde{\theta}$ are the new coordinates and $\tilde{\theta} = 0$ points in the direction of the source. The anisotropy is then defined as

$$A = \frac{\int d\tilde{\Omega}' \chi(1, \tilde{\theta}) \cos \tilde{\theta}}{\int d\tilde{\Omega}' \chi(1, \tilde{\theta}')}, \quad (\text{S36})$$

as in Eq. 5 of the main text. To evaluate the integrals in Eq. S36 we use a planar approximation for $\chi(\tilde{\rho}, \tilde{\theta})$,

$$\chi(\tilde{\rho}, \tilde{\theta}) = c_1 + c_2 \tilde{z} = c_1 + c_2 \tilde{\rho} \cos \tilde{\theta}, \quad (\text{S37})$$

where c_1 and c_2 are given by Eq. S35 at the surface of the detector,

$$\chi(\tilde{\rho} = 1, \tilde{\theta} = 0) = \chi(\rho = \rho_0 - 1, \theta = 0) = c_1 + c_2, \quad (\text{S38})$$

$$\chi(\tilde{\rho} = 1, \tilde{\theta} = \pi) = \chi(\rho = \rho_0 + 1, \theta = 0) = c_1 - c_2. \quad (\text{S39})$$

Rearranging and solving for c_1 and c_2 we have

$$c_1 = \frac{1}{2}(\chi(\rho = \rho_0 - 1, \theta = 0) + \chi(\rho = \rho_0 + 1, \theta = 0)), \quad (\text{S40})$$

$$c_2 = \frac{1}{2}(\chi(\rho = \rho_0 - 1, \theta = 0) - \chi(\rho = \rho_0 + 1, \theta = 0)). \quad (\text{S41})$$

Plugging in $\rho = \rho_0 - 1$, $\rho = \rho_0 + 1$, and $\theta = 0$ into Eq. S35, we have

$$\chi(\rho_0 - 1, 0) = \frac{\alpha}{\rho_0 - 1} - \varepsilon F, \quad (\text{S42})$$

$$\chi(\rho_0 + 1, 0) = \frac{\alpha}{\rho_0 + 1} - \varepsilon G, \quad (\text{S43})$$

where we have defined F and G as

$$F = \alpha \sum_{\ell}^{\infty} \left(\frac{\ell(2\ell + 1 - 1/\rho_0)}{(\ell + 1)(2\ell + 1)\rho_0^{\ell}(\rho_0 - 1)^{\ell+1}} + \left(\frac{\rho_0 - 1}{\rho_0}\right)^{\ell} - \frac{1}{(2\ell + 2)} \left(\frac{\rho_0 - 1}{\rho_0}\right)^{\ell+1} - \frac{1}{(2\ell + 1)(2\ell + 2)(\rho_0 - 1)\rho_0^{\ell+1}} \right), \quad (\text{S44})$$

$$G = \alpha \sum_{\ell}^{\infty} \left(\frac{\ell(2\ell + 1 - 1/\rho_0)}{(\ell + 1)(2\ell + 1)\rho_0^{\ell}(\rho_0 + 1)^{\ell+1}} + \left(\frac{\rho_0}{\rho_0 + 1}\right)^{\ell} - \frac{1}{(2\ell + 2)} \left(\frac{\rho_0}{\rho_0 + 1}\right)^{\ell+1} - \frac{1}{(2\ell + 1)(2\ell + 2)(\rho_0(\rho_0 + 1))^{\ell+1}} \right). \quad (\text{S45})$$

Performing the infinite series gives

$$F = \alpha \left[\frac{\rho_0^2(\rho_0 - 1)}{\rho_0(\rho_0 - 1) - 1} - \frac{1}{2} \log \rho_0 + \frac{1}{2} \log \left(\frac{\rho_0(\rho_0 - 1) - 1}{\rho_0(\rho_0 - 1)} \right) \right], \quad (\text{S46})$$

$$G = \alpha \left[\frac{(\rho_0 + 1)(\rho_0^2 + \rho_0 - 1) + \rho_0}{\rho_0^2 + \rho_0 - 1} - \frac{1}{2} \log(\rho_0 + 1) + \frac{1}{2} \log \left(\frac{\rho_0^2 + \rho_0 - 1}{\rho_0(\rho_0 + 1)} \right) \right]. \quad (\text{S47})$$

The coefficients c_1 and c_2 now take the form of

$$c_1 = \frac{\alpha \rho_0}{\rho_0^2 - 1} - \varepsilon \frac{1}{2} (F + G), \quad (\text{S48})$$

$$c_2 = \frac{\alpha}{\rho_0^2 - 1} - \varepsilon \frac{1}{2} (F - G). \quad (\text{S49})$$

The integrals in the anisotropy, Eq. S36, can now be evaluated, giving

$$A = \frac{2 + \varepsilon(G - F)(\rho_0^2 - 1)}{3[2\rho_0 - \varepsilon(F + G)(\rho_0^2 - 1)]}, \quad (\text{S50})$$

as in Eq. 6 of the main text.

Noise: Langevin Analysis

Equation S50 in the previous section represents the detected signal of the steady-state concentration. To calculate the noise, we add Langevin terms to Eqs. S1 and S2 and make use of the Wiener-Khinchin theorem. The Wiener-Khinchin theorem shows that the autocorrelation and power spectral density of a signal form a Fourier pair. It can

be used further to show that the time averaged correlation function of a signal, $C_T(t)$, is approximately equal to its power spectrum density, $S(\omega)$, at low frequency divided by the averaging time, T

$$C_T(0) = \frac{S(0)}{T}. \quad (\text{S51})$$

Therefore, the time-averaged variance of the anisotropy is

$$\sigma_A^2 = \frac{S_A(\omega=0)}{T} = \frac{1}{T} \int d\omega' \langle \delta\tilde{A}^*(\omega) \delta\tilde{A}(\omega=0) \rangle. \quad (\text{S52})$$

$\delta\tilde{A}$ represents the fluctuations in the Fourier transform of $A(t)$ and $*$ denotes the complex conjugate. The fluctuations in $A(t)$ in time are by definition

$$\delta A(t) = \frac{\int d\Omega \delta c(a, \theta, t) \cos \theta}{\int d\Omega \bar{c}(a, \theta)}, \quad (\text{S53})$$

where δc represents the fluctuations in the pheromone concentration and \bar{c} is the time average of the pheromone concentration, given by Eqs. S37, S48, and S49 (dropping the tildes for convenience). Denoting the denominator of Eq. S53 as Z , we have

$$Z = \int d\Omega \bar{c}(a, \theta) = (4\pi) \frac{2\alpha\rho_0 - \varepsilon(F+G)(\rho_0^2 - 1)}{2a^3(\rho_0^2 - 1)}. \quad (\text{S54})$$

Taking the Fourier transform of Eq. S53 gives

$$\delta\tilde{A}(\omega) = \frac{1}{Z} \int d\Omega \int \frac{d^3k}{(2\pi)^3} \delta\tilde{c}(\vec{k}, \omega) e^{i(a, \Omega) \cdot \vec{k}} \cos \theta. \quad (\text{S55})$$

Using the plane-expansion

$$e^{i(a, \Omega) \cdot \vec{k}} \cos \theta = 4\pi \sum_{\ell, m} i^\ell j_\ell(ak) Y_{\ell, m}(\Omega) Y_{\ell, m}(\hat{k}) \sqrt{\frac{4\pi}{3}} Y_{1, 0}(\Omega), \quad (\text{S56})$$

where i is the imaginary number and j_ℓ are the spherical Bessel functions. Using the orthogonality properties of the spherical harmonics (Eq. S26), Eq. S55 becomes

$$\delta\tilde{A}(\omega) = \frac{1}{Z} \int \frac{d^3k}{(2\pi)^3} \delta\tilde{c}(\vec{k}, \omega) 4\pi i \cos \theta_k j_1(ak), \quad (\text{S57})$$

where θ_k is polar angle in Fourier space. Taking the complex conjugate and averaging gives

$$\langle \delta\tilde{A}^*(\omega') \delta\tilde{A}(\omega) \rangle = \frac{4}{Z^2 (2\pi)^4} \int d^3k' \cos \theta_{k'} j_1(ak') \int d^3k \cos \theta_k j_1(ak) \langle \delta\tilde{c}^*(k', \omega') \delta\tilde{c}(k, \omega) \rangle. \quad (\text{S58})$$

To solve for $\langle \delta\tilde{c}^*(k', \omega') \delta\tilde{c}(k, \omega) \rangle$ we go back to our original PDE system, with the coordinate system centered on the detector, and with the boundary conditions built in:

$$\dot{b} = D_b \nabla^2 b + \mu \delta^3(\vec{x}) + \eta_b \quad (\text{S59})$$

$$\dot{c} = D_c \nabla^2 c + \nu \delta^3(\vec{x} - r_0 \vec{z}) + \eta_c \quad (\text{S60})$$

The statistics of the noise terms are

$$\langle \eta_b(\vec{x}, t) \eta_b(\vec{x}', t') \rangle = 2D_b \delta(t - t') \vec{\nabla}_x \cdot \vec{\nabla}_{x'} [\bar{b}(\vec{x}) \delta^3(\vec{x} - \vec{x}')] \quad (\text{S61})$$

and

$$\langle \eta_c(\vec{x}, t) \eta_c(\vec{x}', t') \rangle = 2D_c \delta(t - t') \vec{\nabla}_x \cdot \vec{\nabla}_{x'} [\bar{c}(\vec{x}) \delta^3(\vec{x} - \vec{x}')] + k_d \bar{b}(\vec{x}) \bar{c}(\vec{x}) \delta(t - t') \delta^3(\vec{x} - \vec{x}'). \quad (\text{S62})$$

Here, \bar{b} and \bar{c} are the time averages of $b(\vec{x}, t)$ and $c(\vec{x}, t)$ respectively. Letting $b(\vec{x}, t) = \bar{b} + \delta b(\vec{x}, t)$ and $c(\vec{x}, t) = \bar{c} + \delta c(\vec{x}, t)$, Eqs. S59 and S60 become

$$\dot{\delta b} = D_b \nabla^2 \delta b + \eta_b \quad (\text{S63})$$

$$\dot{\delta c} = \nabla^2 \delta c - k_d \bar{b} \delta c - k_d \bar{b} \delta c - k_d \bar{b} \delta c + \eta_c. \quad (\text{S64})$$

In Eq. S64 we have neglected second order terms in time. Taking the Fourier transform of both sides of Eq. S64 and rearranging we have

$$\tilde{\delta c}(\vec{k}, \omega) = \frac{\eta_c - k_d \bar{c} \tilde{\delta b}}{D_b k^2 + k_d \bar{b} - i\omega}. \quad (\text{S65})$$

Taking the complex conjugate of Eq. S64 and averaging gives

$$\langle \tilde{\delta c}^*(\vec{k}', \omega') \tilde{\delta c}(\vec{k}, \omega) \rangle = \frac{\langle \eta_c^* \eta_c \rangle + (k_d \bar{c})^2 \langle \tilde{\delta b}^* \tilde{\delta b} \rangle}{(D_c k'^2 + k_d \bar{b} + i\omega')(D_c k^2 + k_d \bar{b} - i\omega)}. \quad (\text{S66})$$

A similar procedure can be followed for δb giving

$$\langle \tilde{\delta b}(\vec{k}', \omega') \tilde{\delta b}(\vec{k}, \omega) \rangle = \frac{\langle \tilde{\eta}_b^* \tilde{\eta}_b \rangle}{(D_b k'^2 + i\omega')(D_b k^2 - i\omega)}. \quad (\text{S67})$$

Plugging Eqs. S67, S61, and S62 into Eq. S66 gives

$$\langle \tilde{\delta c}^*(\vec{k}', \omega') \tilde{\delta c}(\vec{k}, \omega) \rangle = \frac{(4\pi)^4 \delta^3(\vec{k}' - \vec{k}) [2D_c \bar{c} k^2 + k \bar{c} + 2(k_d \bar{c})^2 D_b \bar{b} k^2 / (D_b^2 k^4 + \omega^2)]}{(D_c k^2 + (k_d \bar{b})^2) + \omega^2}. \quad (\text{S68})$$

We can now solve for σ_A^2 by plugging the above equation into Eq. S58,

$$\sigma_A^2 = \frac{4}{Z^2 T} \int_{-\infty}^{\infty} dk j_1^2(ka) \left[\frac{2D_b D_c \bar{c} k^4 + k_d \bar{b} \bar{c} k^2 + 2(k_d \bar{c})^2 \bar{b}}{D_b (D_c k^2 + k_d \bar{b})^2} \right]. \quad (\text{S69})$$

Defining $u \equiv ka$, using $\bar{b} = \mu/4\pi D_b a$, and recalling that $\varepsilon = k_d \mu a / 4\pi D_b D_c$, Eq. S69 becomes

$$\sigma_A^2 = \frac{4\bar{c}}{Z^2 a D_c T} \int_{-\infty}^{\infty} du j_1^2(u) \left[\frac{2u^4 + \varepsilon u^2 + 2f\varepsilon^2}{(u^2 + \varepsilon)^2} \right] \quad (\text{S70})$$

where $f = \nu/\rho_0\mu$. The above integral can be broken up into three separate integrals which in turn can be solved by integration by parts and contour integrations.

$$I_1 = \int_{-\infty}^{\infty} du j_1^2(u) \frac{2u^4}{(u + i\sqrt{\varepsilon})^2 (u - i\sqrt{\varepsilon})^2} = \frac{\pi [1 + \varepsilon - e^{-2\varepsilon^{1/2}} (1 + 2\varepsilon^{1/2} + 3\varepsilon + 2\varepsilon^{3/2})]}{2\varepsilon^{3/2}} \quad (\text{S71})$$

$$I_2 = \int_{-\infty}^{\infty} du j_1^2(u) \frac{\varepsilon u^2}{(u + i\sqrt{\varepsilon})^2 (u - i\sqrt{\varepsilon})^2} = \frac{\pi [-3 + \varepsilon + e^{-2\varepsilon^{1/2}} (3 + 6\varepsilon^{1/2} + 5\varepsilon + 2\varepsilon^{3/2})]}{4\varepsilon^{3/2}} \quad (\text{S72})$$

$$I_3 = \int_{-\infty}^{\infty} du j_1^2(u) \frac{2f\varepsilon}{(u + i\sqrt{\varepsilon})^2 (u - i\sqrt{\varepsilon})^2} = \frac{\pi f [15 - 9\varepsilon + 4\varepsilon^{3/2} - e^{-2\varepsilon^{1/2}} (15 + 30\varepsilon^{1/2} + 21\varepsilon + 6\varepsilon^{3/2})]}{6\varepsilon^{3/2}}. \quad (\text{S73})$$

To first order in ε ,

$$I_1 + I_2 + I_3 \approx \pi \left(\frac{2}{3} - \varepsilon \frac{2}{5} \right). \quad (\text{S74})$$

Plugging in Eqs. S54 and S74 into Eq. S70 and using $\bar{c} = c_1/a^3 = \nu\rho_0/4\pi D_c a(\rho_0^2 - 1)$, we have the variance in the time-average anisotropy,

$$\sigma_A^2 = \frac{2(\rho_0^2 - 1)}{3\nu T} \left[1 + \varepsilon \left[(F + G) \left(\frac{\rho_0^2 - 1}{\rho_0} \right) - \frac{3}{5} \right] \right], \quad (\text{S75})$$

as in Eq. 7 of the main text.

Noise: Scaling Argument

According to the scaling argument of the main text, the variance of the long-time average of the anisotropy is

$$\sigma_A^2 \sim \frac{a^2}{D_c T (1 + \varepsilon) \bar{n}}, \quad (\text{S76})$$

where

$$\bar{n} = \int d^3 \tilde{\rho} \tilde{\chi}(\tilde{\rho}, \tilde{\theta}) \quad (\text{S77})$$

is the number of pheromone molecules within the volume of the detector. Eq. S77 can be solved using Eq. S37

$$\bar{n} = \frac{4\pi c_1}{3} = \frac{4\pi(2\alpha\rho_0 - \varepsilon(F + G)(\rho_0^2 - 1))}{6(\rho_0^2 - 1)}. \quad (\text{S78})$$

Plugging Eq. S78 into Eq. S76 and using $\alpha = \nu a^2 / 4\pi D_c$ we have

$$\sigma_A^2 \sim \frac{3(\rho_0^2 - 1)}{\nu T \rho_0 (1 + \varepsilon) [1 - \varepsilon(F + G)(\rho_0^2 - 1)/(2\rho_0)]}. \quad (\text{S79})$$

To first order in ε , the variance is

$$\sigma_A^2 \sim \frac{3(\rho_0^2 - 1)}{\nu T \rho_0} \left[1 + \varepsilon \left(\frac{1}{2}(F + G) \left(\frac{\rho_0^2 - 1}{\rho_0} \right) - 1 \right) \right]. \quad (\text{S80})$$

Comparing Eq. S80 with Eq. S75, we see that the two expressions agree apart from numerical factors, as stated in the main text.

Information Bounds

Here we prove that the reduced model satisfies the bound $I[s; q'] \geq I[s; A]$, but not the bound $I[s; q] \geq I[s; q']$. Here $s \in \{-1, 1\}$ is the source location, $q = (\ell, r) \in \{(0, 0), (0, 1), (1, 0), (1, 1)\}$ are the pheromone occupancies without degradation, q' are the pheromone occupancies with degradation, and $A \in \{-1, 0, 1\}$ is the anisotropy.

To prove the first bound, we recognize that the information between source and degraded profile is

$$I[s; q'] = \sum_{s\ell r} p_{\ell r|s} p_s \log \frac{p_{\ell r|s}}{\sum_{s'} p_{\ell r|s'} p_{s'}} \quad (\text{S81})$$

$$= \frac{1}{2} \sum_{\ell r} p_{\ell r|-1} \log \frac{2p_{\ell r|-1}}{p_{\ell r|-1} + p_{\ell r|1}} + \frac{1}{2} \sum_{\ell r} p_{\ell r|1} \log \frac{2p_{\ell r|1}}{p_{\ell r|-1} + p_{\ell r|1}}, \quad (\text{S82})$$

where the second step applies $p_s = 1/2$. We introduce the shorthand

$$\begin{aligned} p_{00|1} &\equiv a, & p_{00|-1} &= a, \\ p_{01|1} &\equiv b, & p_{01|-1} &= -b, \\ p_{10|1} &\equiv c, & p_{10|-1} &= -c, \\ p_{11|1} &\equiv d, & p_{11|-1} &= d, \end{aligned} \quad (\text{S83})$$

where the second column follows from the antisymmetry of the solution upon swapping the source location. Inserting Eq. S83 into Eq. S82 and simplifying obtains

$$I[s; q'] = b \log \frac{2b}{b+c} + c \log \frac{2c}{b+c}. \quad (\text{S84})$$

The information between source and anisotropy is

$$I[s; A] = \sum_{sA} \tilde{p}_{A|s} p_s \log \frac{\tilde{p}_{A|s}}{\sum_{s'} \tilde{p}_{A|s'} p_{s'}} \quad (\text{S85})$$

$$= \frac{1}{2} \sum_A \tilde{p}_{A|-1} \log \frac{2\tilde{p}_{A|-1}}{\tilde{p}_{A|-1} + \tilde{p}_{A|1}} + \frac{1}{2} \sum_A \tilde{p}_{A|1} \log \frac{2\tilde{p}_{A|1}}{\tilde{p}_{A|-1} + \tilde{p}_{A|1}}, \quad (\text{S86})$$

where for clarity we have used a tilde to distinguish the anisotropy distribution $\tilde{p}_{A|s}$ from the profile distribution $p_{\ell r|s}$. Given the relationship $A = \ell - r$, we have

$$\begin{aligned} \tilde{p}_{-1|1} &= p_{01|1} = b, & \tilde{p}_{-1|-1} &= p_{01|-1} = -b, \\ \tilde{p}_{0|1} &= p_{00|1} + p_{11|1} = a + d, & \tilde{p}_{0|-1} &= p_{00|-1} + p_{11|-1} = a + d, \\ \tilde{p}_{1|1} &= p_{10|1} = c, & \tilde{p}_{1|-1} &= p_{10|-1} = -c. \end{aligned} \quad (\text{S87})$$

Inserting Eq. S87 into Eq. S86 and simplifying obtains

$$I[s; A] = b \log \frac{2b}{b+c} + c \log \frac{2c}{b+c}. \quad (\text{S88})$$

Because Eqs. S84 and S88 are identical, we conclude that $I[s; q'] = I[s; A]$. That is, the reduced model satisfies the first bound $I[s; q'] \geq I[s; A]$ by equality.

The violation of the second bound can now be shown by counterexample. We see from Fig. 3C that $I[s; A]$ with degradation ($\epsilon > 0$) can be larger than without degradation ($\epsilon = 0$). Because we just found that $I[s; A] = I[s; q']$, we therefore conclude that $I[s; q']$ with degradation can be larger than without degradation—which we denoted $I[s; q]$. This example thus shows that the second bound $I[s; q] \geq I[s; q']$ does not generally hold.